

Article

Heterogeneous Bimetallic Cu–Ni Nanoparticle-Supported Catalysts in the Selective Oxidation of Benzyl Alcohol to Benzaldehyde

Lili Liu * , Xiaojing Zhou, Li Liu , Shuai Jiang, Yingjie Li, Luxia Guo, Shijuan Yan and Xishi Tai * 

School of Chemistry & Chemical Engineering and Environmental Engineering, Weifang University, Weifang 261061, China; zhouxiaojing105@wfu.edu.cn (X.Z.); liuliwfu@126.com (L.L.); j_s9908@foxmail.com (S.J.); liyingjie1999@foxmail.com (Y.L.); glx08070111@foxmail.com (L.G.); ysj1714960527@foxmail.com (S.Y.)

* Correspondence: liulili122@wfu.edu.cn (L.L.); taixs@wfu.edu.cn (X.T.);

Tel.: +86-536-878-5283 (L.L.); +86-536-878-5363 (X.T.)

Received: 10 May 2019; Accepted: 12 June 2019; Published: 17 June 2019



Abstract: Three bimetallic Cu–Ni nanoparticle-supported catalysts were synthesized by co-immobilization followed by H₂ reduction. A chromium(III) terephthalate metal organic framework (MIL-101), titanium dioxide (TiO₂), and carbon (C) with different properties (acidity and Brunauer–Emmett–Teller surface area) were selected as supports for studying the effect of the support nature on the catalytic activity and selectivity in the oxidation of benzyl alcohol. The physicochemical properties of the Cu–Ni-supported catalysts were characterized by XRD, NH₃-TPD, nitrogen adsorption/desorption, TEM, EDS, XPS, and ICP-OES. Bimetallic Cu–Ni nanoparticles were highly dispersed on the support. The catalytic activities of CuNi/MIL-101, CuNi/TiO₂, and CuNi/C were tested in the selective oxidation of benzyl alcohol to benzaldehyde in the presence of molecular oxygen under mild reaction conditions. The highest benzaldehyde yields were achieved with CuNi/TiO₂, CuNi/MIL-101, and CuNi/C catalysts at 100 °C within 4 h under 5, 3, and 3 bar of O₂, respectively. The bimetallic Cu–Ni-supported catalysts possessed two types of catalytic active sites: acid sites and bimetallic Cu–Ni nanoparticles. The CuNi/MIL-101 catalyst possessed a high number of acid sites and exhibited high yield during selective benzyl alcohol oxidation to benzaldehyde. Importantly, the catalysts exhibited a high functional group (electron-donating and electron-withdrawing groups) tolerance. Cu–Ni-supported catalysts with an Cu:Ni mole ratio of 1:1 exhibited the highest yield of 47% for the selective oxidation of benzyl alcohol to benzaldehyde. Reusability and leaching experiment results exhibited that CuNi/MIL-101 showed better stability than CuNi/TiO₂ and CuNi/C catalysts due to the large porous cavities of MIL-101 support; these cavities can be used to trap bimetallic Cu–Ni nanoparticles and inhibit nanoparticle leaching.

Keywords: Cu–Ni nanoparticles; MIL-101; TiO₂; carbon; benzyl alcohol oxidation

1. Introduction

Benzaldehyde is a valuable precursor for the production of perfumes, pharmaceuticals, dyestuffs, and agrochemicals [1]. Conventionally, benzaldehyde is synthesized by the selective oxidation of benzyl alcohol in the presence of inorganic oxidants such as KMnO₄, CrO₃, MnO₂, and Br₂ [2]. However, these reagents may produce high amounts of waste and hazardous/toxic compounds during selective oxidation, which may result in intensive environmental problems [3]. Therefore, developing green catalytic processes under mild conditions is necessary to produce clean benzaldehyde by benzyl alcohol oxidation.

Recently, supported noble metals, such as Au, Pd, Ru, Au–Pd, Au–Ag, and Au–Ni, have been reported to exhibit high catalytic activities in selective oxidation of benzyl alcohol to benzaldehyde under mild conditions [4–11]. However, these noble metals, as limited resources, are expensive. On the other hand, non-noble metal-supported catalysts may be an alternative to noble metals for the selective oxidation of benzyl alcohol [12]. Cruz et al. [12] reported that copper and copper oxide nanoparticles supported on SBA-15 showed good catalytic activity and selectivity in the selective oxidation of benzyl alcohol to benzaldehyde. Fu et al. [13] revealed that Ni–Co bimetallic oxide nanoparticles supported on N-doped FDU-15 featured high benzyl alcohol conversion (93.4%) and excellent benzaldehyde selectivity (97.8%) when air was used as the oxidant at 110 °C. Bimetallic Cu–Ni nanoparticles supported on activated carbon also showed good catalytic performance with a 46.8% conversion for benzyl alcohol oxidation to benzaldehyde using hydrogen peroxide as the oxidizing agent at 80 °C within 2 h in toluene [14]. Thus, the development of selective oxidation catalytic processes using inexpensive metals such as Cu, Cu–Ni, and Ni–Co, is vital for achieving economic efficiency.

Metal–organic frameworks (Cu(II)-MOF-101 ZIF-8, and MIL-101), metal oxides (TiO₂, Al₂O₃, MgO, and MnO₂), and carbon (C) are widely used as the support for the selective oxidation of alcohols [4,9–11,14–17]. To optimize the performance of catalysts, it is essential to understand the effect of the support on the catalytic activity for the selective oxidation reaction [18]. However, the effect of the acidity and surface properties of the support on the catalytic performance has not investigated in detail. Thus in this work, bimetallic Cu–Ni nanoparticles supported on a representative chromium(III) terephthalate metal organic framework MIL-101, TiO₂, and C were synthesized by co-immobilization followed by H₂ reduction. The catalytic activities of CuNi/MIL-101, CuNi/TiO₂, and CuNi/C were studied for the oxidation of benzyl alcohol to benzaldehyde using molecular oxygen (O₂) as the green oxidant. The reaction conditions such as type of solvent, reaction time, reaction pressure, and reaction temperature were optimized in the selective oxidation of benzyl alcohol in the presence of bimetallic Cu–Ni supported-catalysts. Furthermore, we attempted to establish the relationship between the catalytic performance and properties of the supports. The scope of substances and stability of catalysts in selective oxidation were also investigated.

2. Results and Discussion

2.1. Catalyst Synthesis and Characterization

We selected a chromium(III) terephthalate metal organic framework MIL-101, TiO₂, and C as supports to study the effect of support nature on the catalytic activity and selectivity in benzyl alcohol oxidation. MIL-101 was synthesized by a hydrothermal method at 220 °C for 18 h by using chromium(III) nitrate nonahydrate (Cr(NO₃)₃·9H₂O), terephthalic acid, and deionized water without the addition of toxic and corrosive hydrofluoric acid [19]. The as-synthesized MIL-101 was further purified using hot ethanol at 90 °C to remove the remaining unreacted terephthalic acid trapped in the pores and dried subsequently in a vacuum oven at 150 °C for 12 h to remove the terminal water molecules. The purchased TiO₂ and C were used as received without any further modification. The physicochemical properties of the supports and Cu–Ni-supported catalysts were determined and are summarized in Table 1. Figure 1 shows the adsorption–desorption isotherms of nitrogen for the supports and Cu–Ni-supported catalysts. All samples exhibited a typical type IV isotherm. The MIL-101 and C samples presented a hysteric loop due to capillary condensation, which is representative of porous materials [20]. The Brunauer–Emmett–Teller (BET) surface areas of MIL-101, TiO₂, and C were measured as 1186.0, 15.2, and 94.9 m²/g, respectively. The trend of BET surface areas for the supports follows the order MIL-101 > C > TiO₂. The BET surface areas of CuNi/MIL-101, CuNi/TiO₂, and CuNi/C were determined to be 1119.2, 8.5 and 55.6 m²/g, respectively. Notably, the surface area of the Cu–Ni-supported catalysts decreased significantly when compared with that of MIL-101, TiO₂, and C due to the immobilization of the Cu–Ni nanoparticles inside the pores. Similar

results have been observed in other samples after the immobilization of metal nanoparticles [10,19]. The total pore volume calculated by the Barrett Joyer Halenda model from the nitrogen desorption isotherm reached 0.49, 0.45, 0.014, 0.0078, 0.11, and 0.079 cm³/g for MIL-101, CuNi/MIL-101, TiO₂, CuNi/TiO₂, C, and CuNi/C, respectively. The corresponding mean pore diameters were 2.8, 2.5, 4.3, 4.7, 4.6, and 5.2 nm for MIL-101, CuNi/MIL-101, TiO₂, CuNi/TiO₂, C, and CuNi/C, respectively. Ammonia temperature programmed desorption (NH₃-TPD) was used to measure the acidic properties of the MIL-101, TiO₂, and C supports, and the results are shown in Figure 2. Three peaks were observed on the spectra of MIL-101 in the range of 40 °C–600 °C, whereas one broad peak was observed on the spectra of TiO₂ and C. The low-temperature desorption peak centered at approximately 270 °C was attributed to adsorbed NH₃ on Lewis acid sites, whereas the high-temperature desorption peak at approximately 340 °C was assigned to Brønsted acid sites [21–25]. TiO₂ contained only Brønsted acid sites, C mainly possessed Lewis acid sites, and MIL-101 preliminarily included Lewis and Brønsted acid sites. For MIL-101, the peak at 443.8 °C was attributed to its structural decomposition. MIL-101 contained more adsorption sites for NH₃ than TiO₂ and C. The numbers of Lewis and Brønsted acid centers located at 264.6 °C and 361.7 °C for MIL-101 reached 0.705 and 3.308 mmol/g, respectively. However, extremely low peaks at 336.1 °C and 275.6 °C were noted in the NH₃-TPD curves of TiO₂ and C, with the amounts of acid sites reaching 0.062 and 0.039 mmol/g, respectively. CuNi/MIL-101, CuNi/TiO₂, and CuNi/C catalysts were prepared by a co-immobilization method, followed by treatment with a stream of H₂ (12 mL/min) for 2 h at 50 °C. Figure 3 shows the x-ray diffraction (XRD) patterns of MIL-101, CuNi/MIL-101, TiO₂, CuNi/TiO₂, C, and CuNi/C. MIL-101 and CuNi/MIL-101 presented similar XRD patterns (Figure 3a), thereby proving the preservation of the crystal structures of MIL-101 after loading of the Cu–Ni nanoparticles [26,27]. Based on the XRD patterns, only the rutile phase was observed in TiO₂ (Figure 3b) [28,29]. The main diffraction peak of TiO₂ was revealed at 2θ = 27.7°, which represents the rutile (110) phase [28]. The XRD patterns of TiO₂ showed no peak corresponding to the anatase (101) phase at 2θ = 25.3° [29]. As shown in the XRD patterns of TiO₂, other diffraction peaks appeared at 2θ = 36.4°, 39.5°, 41.6°, 44.4°, 54.7°, 57.0°, 63.1°, 64.3°, 69.2°, 70.1°, and 76.9°, which were consistent with the rutile phase of TiO₂. By comparing the XRD pattern of CuNi/TiO₂ with that of TiO₂, the CuO and NiO nanoparticle loading introduced no significant changes in the TiO₂ structure (Figure 3b). The lattice plane of graphite (JCPDS, File No. 74-2330) was noted in Figure 3c. The characteristic peak at 2θ = 24.8° in the XRD patterns was associated with the (002) of carbon support (Figure 3c) [30–32]. Furthermore, characteristic CuO and NiO peaks were absent in the XRD patterns of CuNi/TiO₂ and CuNi/C due to the low amounts of Cu and Ni in the catalysts [33,34].

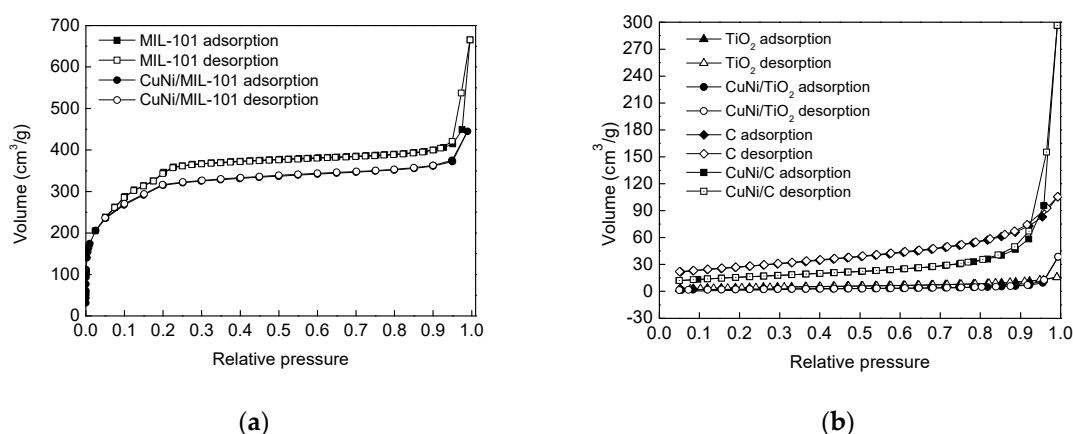
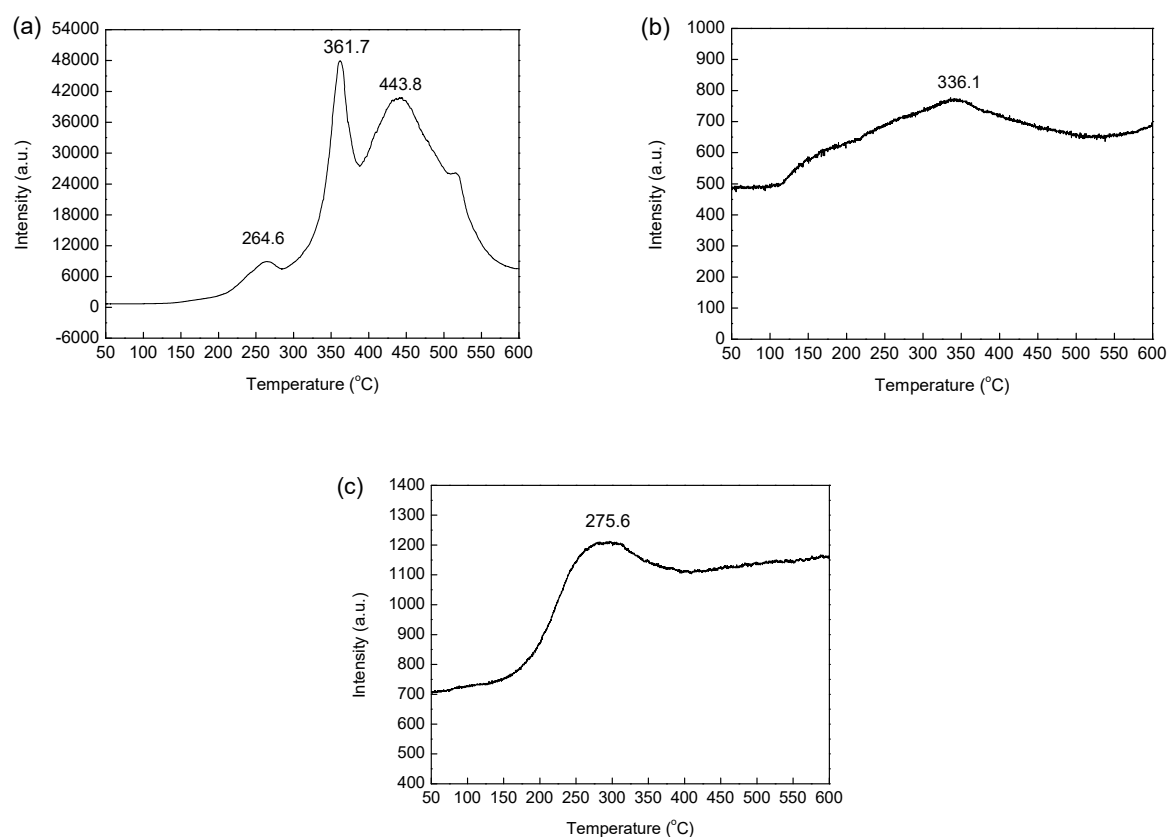


Figure 1. Nitrogen adsorption–desorption isotherms of the samples measured at 77 K: (a) The nitrogen–adsorption of MIL-101 and CuNi/MIL-101; (b) The nitrogen–adsorption of TiO₂, CuNi/TiO₂, C, and CuNi/C.

Table 1. The physicochemical properties of supports and the as-prepared Cu-Ni-supported catalysts.

Entry	Samples	BET Surface Area (m ² /g)	Pore Volume (cm ³ /g)	Pore Diameter (nm)
1	MIL-101	1186.0	0.49	2.8
2	CuNi/MIL-101	1119.2	0.45	2.5
3	TiO ₂	15.2	0.014	4.3
4	CuNi/TiO ₂	8.5	0.0078	4.7
5	C	94.9	0.11	4.6
6	CuNi/C	55.6	0.079	5.2

**Figure 2.** The NH₃-TPD curves of MIL-101 (a); TiO₂ (b); and C (c).

We conducted XPS measurements to investigate the chemical state of Cu and Ni in the CuNi/MIL-101, CuNi/TiO₂, and CuNi/C catalysts. Figure 4 shows the Cu 2p and Ni 2p XPS spectra of the as-prepared CuNi/MIL-101, CuNi/TiO₂, and CuNi/C catalysts. For all of the catalysts, two peaks at 932.5 and 952.5 eV were attributed to Cu 2p_{3/2} and Cu 2p_{1/2}, respectively, thereby suggesting the presence of Cu²⁺ in the catalysts [35]. Furthermore, two satellite peaks of Cu 2p_{3/2} and Cu 2p_{1/2} were detected, thereby further confirming the existence of Cu²⁺ [36,37]. The oxidized Ni of Ni²⁺ 2p_{3/2} and Ni²⁺ 2p_{1/2} were detected at the binding energies of 856.6 and 874.0 eV, respectively, in the Ni 2p spectra of CuNi/MIL-101, CuNi/TiO₂, and CuNi/C possibly due to oxidation of the catalysts exposed to air [11,38]. The peaks at 861.8 and 880.2 eV were assigned to satellites in all the catalysts [39].

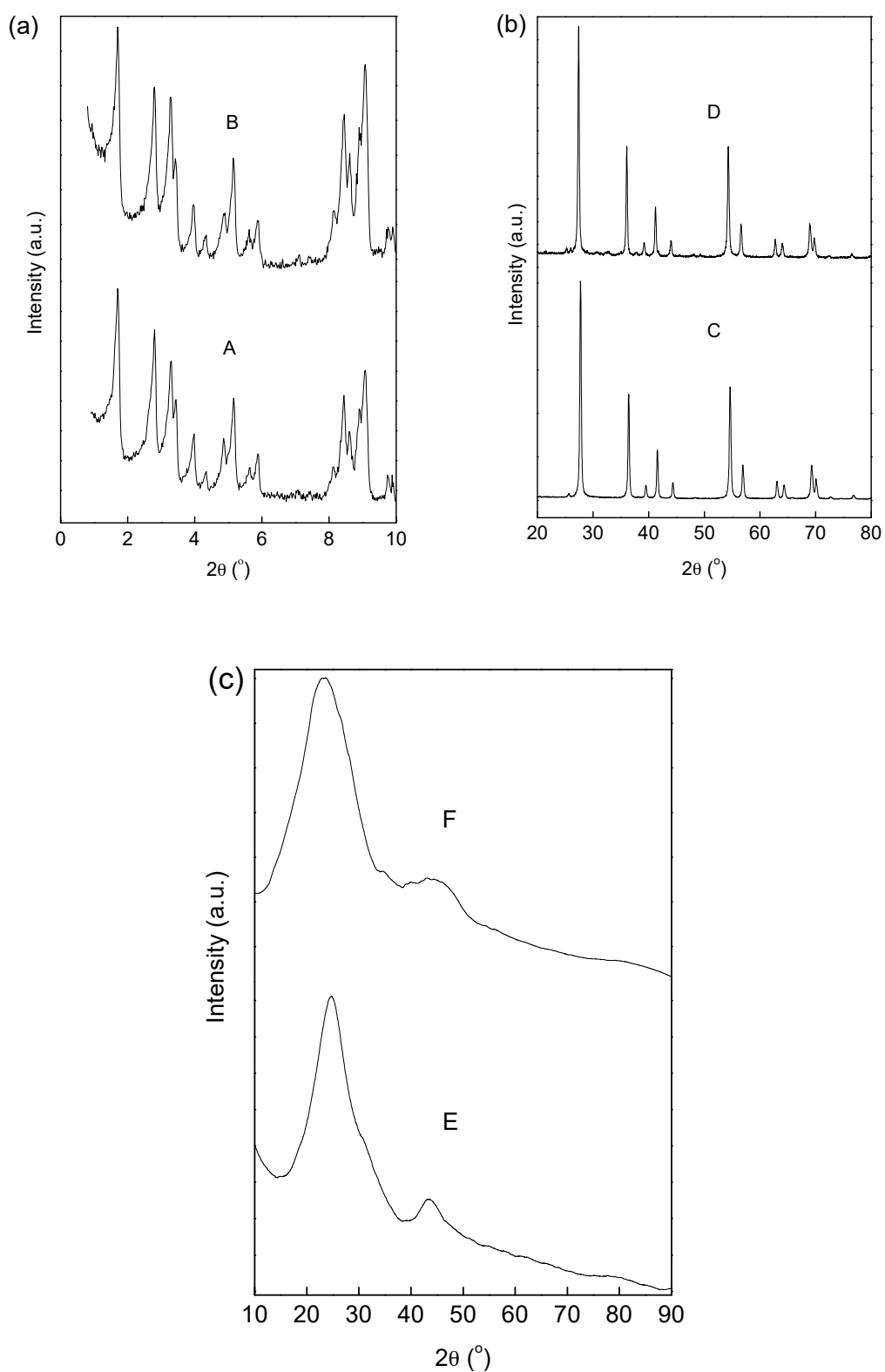


Figure 3. (a) XRD patterns of MIL-101 (A) and CuNi/MIL-101 (B); (b) XRD patterns of TiO_2 (C) and CuNi/ TiO_2 (D); (c) XRD patterns of C (E) and CuNi/C (F).

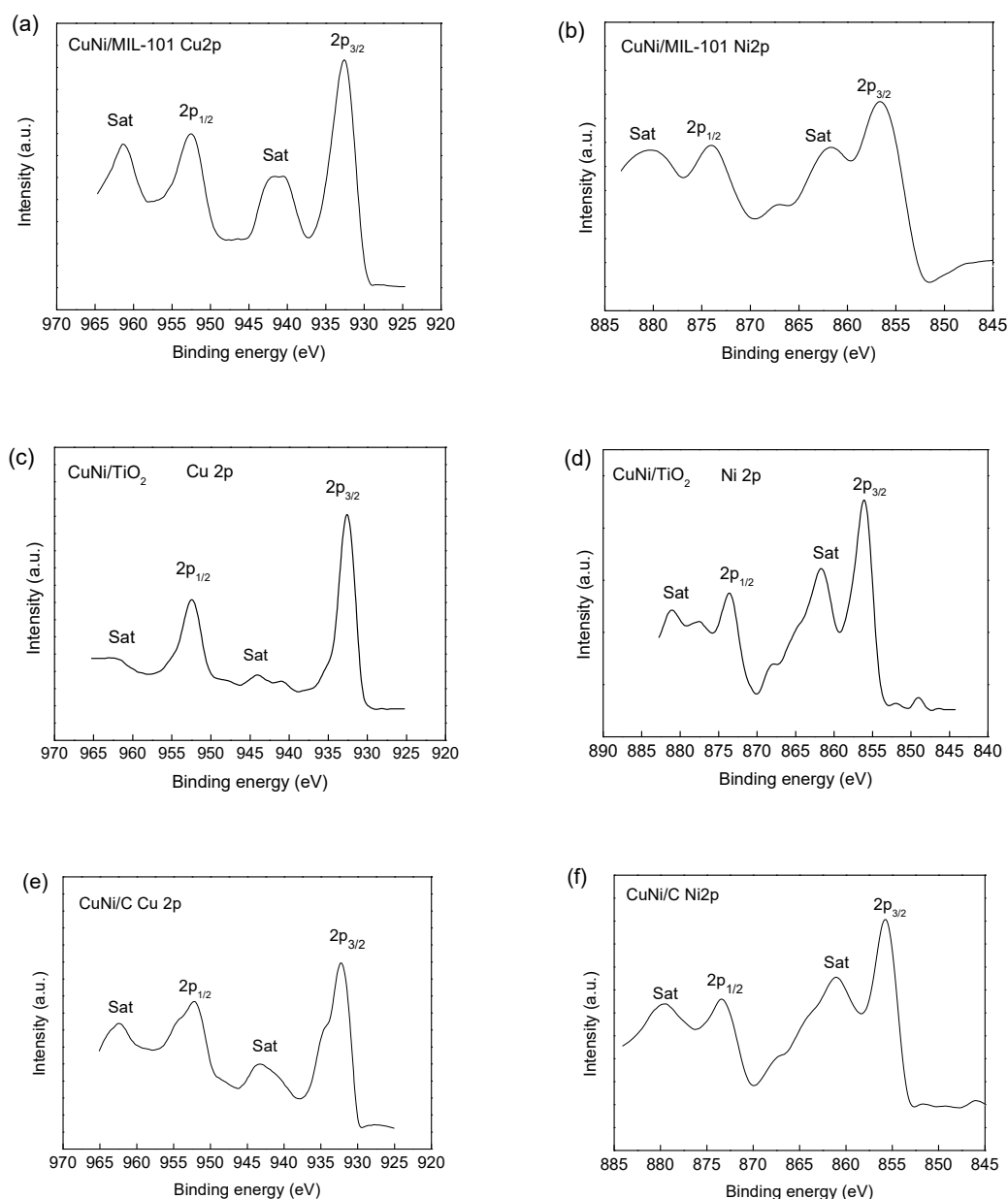


Figure 4. XPS spectra of CuNi/MIL-101 (a,b), CuNi/TiO₂ (c,d), and CuNi/C (e,f).

The morphology of the as-synthesized CuNi/MIL-101 catalyst obtained via co-immobilization followed by H₂ reduction was determined by transmission electron microscope (TEM) (Figure 5a–c). Line scanning analysis of CuNi/MIL-101 was also determined via energy dispersive x-ray spectrometry (EDS), as observed in Figure 5d. The CuNi/MIL-101 catalyst exhibited a micro sized but well-defined cuboidal morphology. EDS line scanning profiles revealed that Cu and Ni were homogeneously distributed throughout the entire MIL-101, thereby indicating the formation of a CuNi alloy structure. The morphology of the CuNi/TiO₂ and CuNi/C catalysts was characterized by TEM. Figure 6 displays the TEM images of CuNi/TiO₂ and CuNi/C. Figure 6 indicates that the CuNi/TiO₂ particles aggregated, but exhibited remarkable rutile structures and grain interfaces. The TEM image of CuNi/C showed that the catalyst exhibited the morphology of spherical particles with a mean diameter size of 10–30 nm (Figure 6).

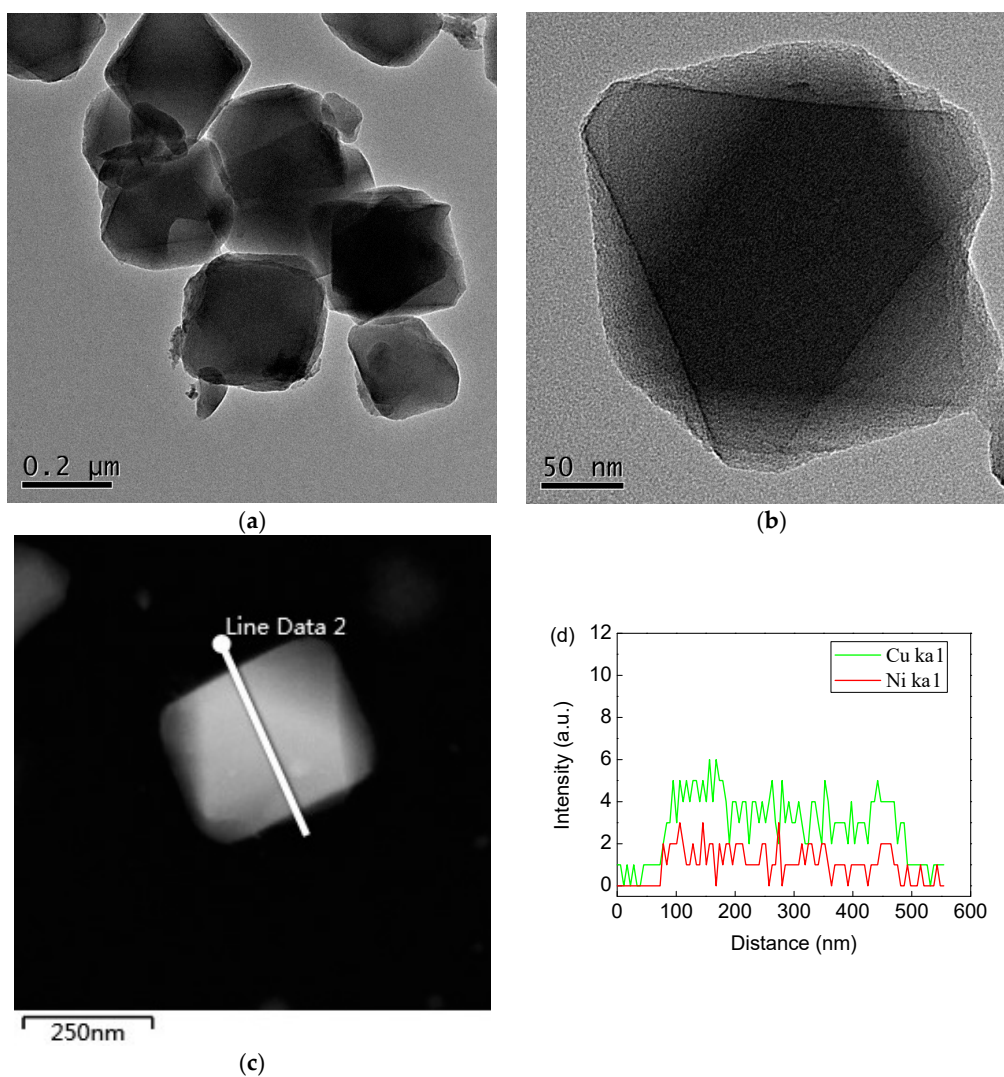


Figure 5. TEM images (a–c) and EDS line-scanning profile analysis of typical nanoparticles indicated by the white line in (c) for CuNi/MIL-101 (d).

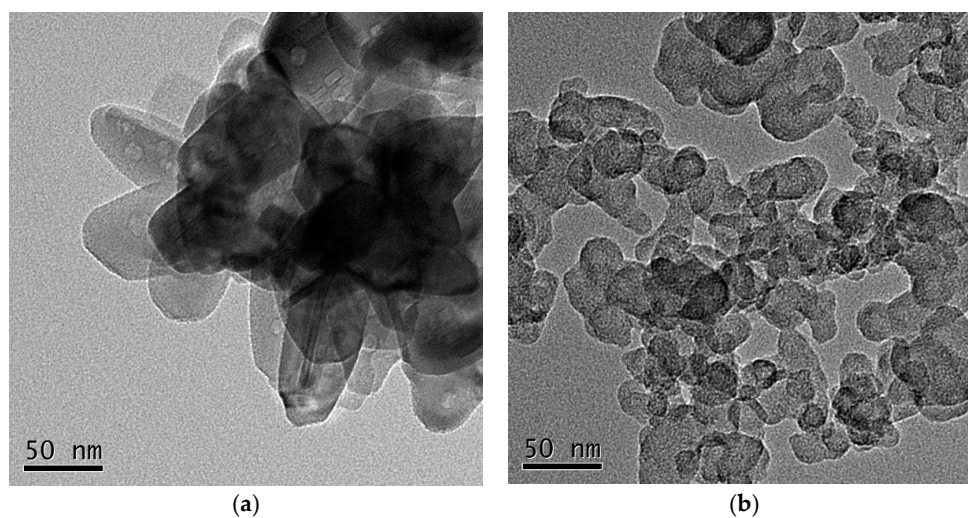


Figure 6. TEM images of CuNi/TiO₂ (a) and CuNi/C (b).

2.2. Benzyl Alcohol Oxidation Using Cu–Ni Bimetallic Catalysts

The catalytic activities of the as-prepared Cu–Ni-supported catalysts for benzyl alcohol oxidation were determined with molecular oxygen as a green oxidant. To avoid producing benzoic acid and benzyl benzoate, we conducted a series of reactions to obtain the optimal reaction conditions to produce benzaldehyde. First, the effects of reaction time on benzyl alcohol conversion, benzaldehyde selectivity, and yield of the CuNi/TiO₂, CuNi/MIL-101, and CuNi/C catalysts were studied. The oxidation reaction was kept at 100 °C under 5 bar of O₂, and the results are presented in Figure 7. For all of the catalysts, the conversion of benzyl alcohol increased with the prolonged reaction time. However, the selectivity of benzaldehyde decreased at a reaction time above 2 h. The yields of benzaldehyde did show an increase after the reaction time reached up to 4 h for the CuNi/TiO₂, CuNi/MIL-101, and CuNi/C catalysts, therefore, the optimal reaction time was set at 4 h for all of the catalysts. Maximum yields of 32.7%, 41.5%, and 34.8% were obtained within 4 h for CuNi/TiO₂, CuNi/MIL-101, and CuNi/C, respectively. CuNi/MIL-101 presented a higher benzaldehyde yield than CuNi/TiO₂ and CuNi/C. The acidity of the support substantially influenced the product selectivity. According to the NH₃-TPD measurement, the values of the acid sites for MIL-101, TiO₂, and C reached 4.013, 0.062, and 0.039 mmol/g, respectively. The highest yield was observed in CuNi/MIL-101, which contained more acid sites in benzyl alcohol oxidation to benzaldehyde, in accordance with previously reported results [11,14]. Benzaldehyde selectivity was lower in the base *N,N*-dimethylformamide (DMF) than in the THF and 1,4-dioxane solvents over the AuNi/MIL-101-1 catalyst [11]. The acid sites of the supports also played a crucial role in benzyl alcohol oxidation. A blank experiment showed that benzyl alcohol conversions reached 25.8%, 13.6%, and 12.9% at 100 °C under 5 bar of O₂ within 4 h over the MIL-101, TiO₂, and C supports, respectively (Table 1, entries 1–3). MIL-101 with more acid sites showed higher catalytic activity than TiO₂ and C. Notably, the conversions of benzyl alcohol amounted to 54.9%, 62.8%, and 64.3% at 100 °C under 5 bar of O₂ within 4 h for CuNi/TiO₂, CuNi/MIL-101, and CuNi/C, respectively. Higher benzyl alcohol conversions were observed for Cu–Ni supported catalysts than the supports (MIL-101, TiO₂, and C) without Cu–Ni particle loading. These results confirm that bimetallic Cu–Ni-supported catalysts possess two types of catalytic active sites: Lewis/Brønsted acid sites and bimetallic Cu–Ni nanoparticles.

Second, conditions such as the type of solvent, reaction pressure, and temperature were optimized in the oxidation of benzyl alcohol in the presence of Cu–Ni bimetallic catalysts under magnetic stirring (500 rpm). Table 1 summarizes the results. Selective oxidation of benzyl alcohol in organic solvents such as dioxane, DMF, acetonitrile, and THF were investigated by CuNi/TiO₂, CuNi/MIL-101, and CuNi/C at 100 °C for 4 h under 5 bar, 3 bar, and 5 bar of O₂. The best catalytic performance was observed in THF (Table 2, entries 4–7, 13–16, and 22–25). Moreover, in the optimization of the reaction temperature of the CuNi/MIL-101, CuNi/TiO₂, and CuNi/C catalysts for the oxidation of benzyl alcohol, benzyl alcohol conversion continuously increased with increasing reaction temperature from 80 °C to 120 °C, along with a decreased benzaldehyde selectivity as oxidation is usually endothermic; thus, deep oxidation of benzaldehyde to benzoic acid easily occurred at high reaction temperatures (Table 2, entries 7–9, 16–18, and 26–28) [40]. The highest yield was obtained at 100 °C for all catalysts (Table 2, entries 7–9, 16–18, and 26–28). Oxidation of benzyl alcohol was conducted with different reaction pressures (1–7 bar) to determine the proper reaction pressure for Cu–Ni bimetallic catalysts (Table 2, entries 7, 10–12, 16, 19–20, 25, and 28–30). Increasing the reaction pressure can increase the conversion of benzyl alcohol. However, the selectivity to benzaldehyde decreased due to the appearance of over-oxidized products [41,42]. The highest yields of benzaldehyde were achieved in the CuNi/TiO₂, CuNi/MIL-101, and CuNi/C catalysts at 100 °C under 5, 3, and 3 bar of O₂, respectively. Further increasing the reaction pressure to 7 bar of O₂ caused no substantial increase in benzyl alcohol conversion, but significantly decreased the selectivity to benzaldehyde for the CuNi/MIL-101 and CuNi/C catalysts (Table 2, entries 12, 21, and 30).

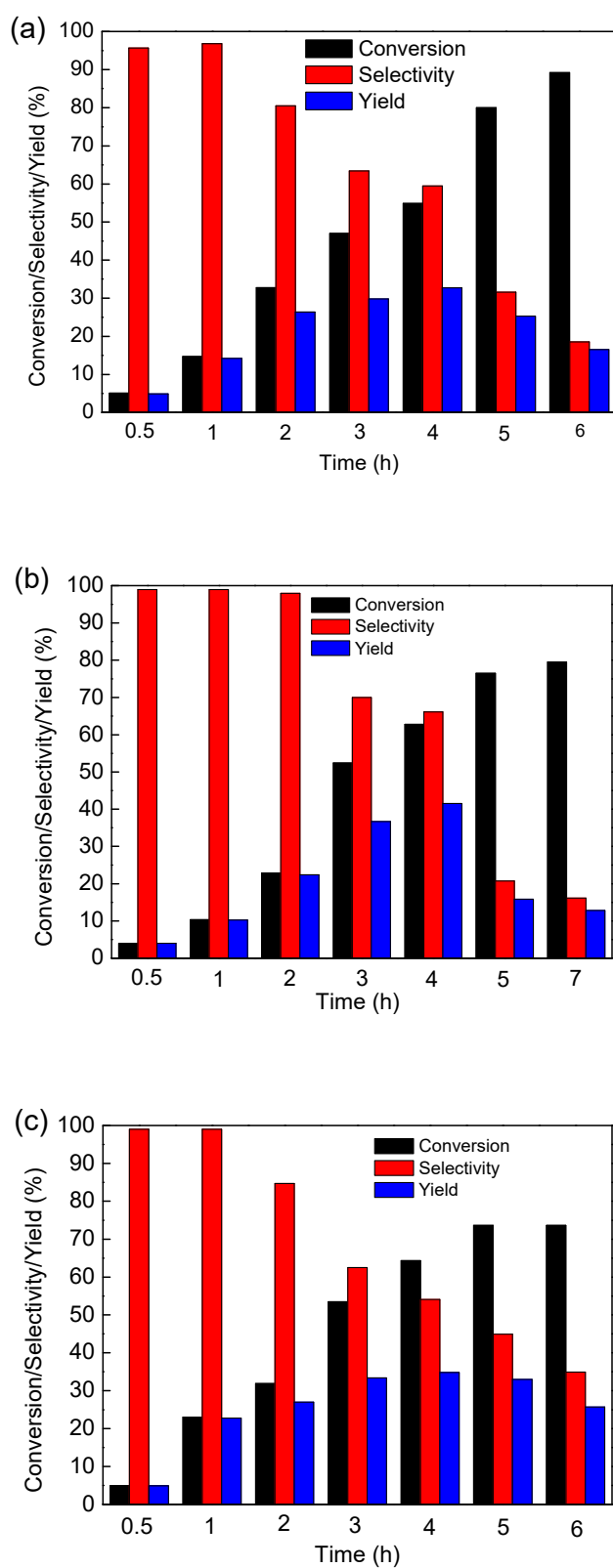


Figure 7. The oxidation of benzyl alcohol with the reaction time of the catalysts: (a) CuNi/TiO₂; (b) CuNi/MIL-101; (c) CuNi/C (reaction condition: benzyl alcohol (0.2 mmol), THF (1.5 mL), catalyst (40 mg), 100 °C, 5 bar).

Table 2. The catalytic activity of the catalyst in the selective oxidation of benzyl alcohol to benzaldehyde ¹.

Entry	Catalyst	Solvent	T (°C)	Pressure (bar)	Con. (%) ²	Sel. (%) ²	Yield (%)
1	MIL-101	THF	100	5	25.8	94.2	24.3
2	TiO ₂	THF	100	5	13.6	83.3	11.3
3	C	THF	100	5	12.9	98.0	12.6
4	CuNi/TiO ₂	dioxane	100	5	4.6	98.4	4.5
5	CuNi/TiO ₂	DMF	100	5	2.9	98.1	2.8
6	CuNi/TiO ₂	acetonitrile	100	5	3.7	98.3	3.6
7	CuNi/TiO ₂	THF	100	5	54.9	59.5	32.7
8	CuNi/TiO ₂	THF	80	5	5.0	99.0	5.0
9	CuNi/TiO ₂	THF	120	5	86.2	15.3	13.2
10	CuNi/TiO ₂	THF	100	1	42.8	73.7	31.5
11	CuNi/TiO ₂	THF	100	3	47.5	63.9	30.4
12	CuNi/TiO ₂	THF	100	7	78.1	20.9	16.3
13	CuNi/MIL-101	dioxane	100	3	24.6	95.0	23.4
14	CuNi/MIL-101	DMF	100	3	2.0	99.0	2.0
15	CuNi/MIL-101	acetonitrile	100	3	10.1	98.2	9.9
16	CuNi/MIL-101	THF	100	3	55.4	84.8	47.0
17	CuNi/MIL-101	THF	80	3	42.0	98.0	41.2
18	CuNi/MIL-101	THF	120	3	69.3	64.8	44.9
19	CuNi/MIL-101	THF	100	1	34.1	99.0	33.8
20	CuNi/MIL-101	THF	100	5	62.8	66.1	41.5
21	CuNi/MIL-101	THF	100	7	68.6	43.7	33.4
22	CuNi/C	dioxane	100	5	30.9	94.3	29.1
23	CuNi/C	DMF	100	5	6.8	97.4	6.6
24	CuNi/C	acetonitrile	100	5	28.4	95.3	27.1
25	CuNi/C	THF	100	5	64.3	54.1	34.8
26	CuNi/C	THF	80	3	34.5	88.4	30.5
27	CuNi/C	THF	100	3	57.6	68.5	39.5
28	CuNi/C	THF	120	3	63.5	45.2	28.7
29	CuNi/C	THF	100	1	27.4	98.0	26.9
30	CuNi/C	THF	100	7	64.4	43.5	28.0

¹ Reaction conditions: benzyl alcohol (0.2 mmol), solvent (1.5 mL), catalyst (40 mg), 4 h. ² Determined by GC.

To examine the scope of the selective oxidation reaction, we extended the catalytic protocol to other alcohols including 4-methylbenzyl alcohol, 4-methoxybenzyl alcohol, 4-chlorobenzyl alcohol, and n-butanol, the results of which are listed in Table 3. Aromatic alcohols including those bearing functional groups such as alkoxy, alkyl, and chloro were converted to the corresponding aldehydes, and afforded good catalytic activity in the selective oxidation reaction (Table 3, entries 1–3). Conversions of 4-methylbenzyl alcohol, 4-methoxybenzyl alcohol, and 4-chlorobenzyl alcohol were 73.8%, 87.9%, and 87.3% at 100 °C under 5 bar of O₂ within 4 h, respectively (Table 3, entries 1–3). The selectivities of the aldehydes reached 24.4%, 28.3%, and 25.2% when 4-methylbenzyl alcohol, 4-methoxybenzyl alcohol, and 4-chlorobenzyl alcohol were used, respectively (Table 3, entries 1–3). The experimental data showed that the functional groups including electron-donating (alkoxy and alkyl) and electron-withdrawing (chloro) groups on the phenyl ring resulted in negligible effects on the conversions and selectivities (Table 3, entries 1–3). n-Butanol as the linear alcohol was also successfully oxidized to the corresponding compounds. The conversion and selectivity of n-butyl aldehyde reached 74.9% and 26.2%, respectively (Table 3, entry 4).

Table 3. Catalytic activities of CuNi/MIL-101 for the oxidation of various alcohols ¹.

Entry	Substrates	Products	Conv. (%)	S (%)
1			73.8	24.4
2			87.9	28.3
3			87.3	25.2
4			74.9	26.2

¹ Reaction conditions: alcohol (0.2 mmol), THF (1.5 mL), CuNi/MIL-101 (0.04 g), 100 °C, 5 bar, 4 h.

The catalytic activity of Cu–Ni-supported catalysts with different Cu:Ni mole ratios for the selective oxidation of benzyl alcohol were also investigated at 100 °C within 4 h under 3 bar of O₂ in THF (Table 4). The results showed that the benzyl alcohol conversion, benzaldehyde selectivity, and yield depended strongly on the mole ratio of Cu:Ni for the oxidation of benzyl alcohol. The yields of benzaldehyde amounted to 33.6%, 42.6%, 47.0%, 36.0%, and 30.3% at 100 °C under 3 bar of O₂ within 4 h for Cu(3)Ni/MIL-101, Cu(2)Ni/MIL-101, CuNi/MIL-101, CuNi(2)/MIL-101, and CuNi(3)/MIL-101, respectively. The highest yield was shown by the CuNi/MIL-101 catalyst, suggesting that Cu–Ni-supported catalysts with a Cu:Ni mole ratio of 1:1 presented its optimal proportion on MIL-101.

Table 4. The catalytic activity of Cu–Ni-supported catalysts in the selective oxidation of benzyl alcohol to benzaldehyde ¹.

Entry	Catalyst	w _{Cu} (%)	w _{Ni} (%)	Cu:Ni Mole Ratio	Conv. (%)	S (%)	Yield (%)
1	Cu(3)Ni/MIL-101	4.45	1.43	3:1	77.6	43.3	33.6
2	Cu(2)Ni/MIL-101	3.96	1.87	2:1	65.4	65.1	42.6
3	CuNi/MIL-101	3.15	2.80	1:1	55.4	84.8	47.0
4	CuNi(2)/MIL-101	2.20	3.77	1:2	72.6	49.6	36.0
5	CuNi(3)/MIL-101	1.62	4.40	1:3	78.2	38.8	30.3

¹ Reaction conditions: benzyl alcohol (0.2 mmol), THF (1.5 mL), catalyst (0.04 g), 100 °C, 3 bar, 4 h.

The reusability of catalysts in the oxidation reaction of benzyl alcohol was tested at 100 °C under 5 bar of O₂ (Figure 8). A slight decrease in catalytic activity occurred after the fourth run, thereby demonstrating the good stability of CuNi/MIL-101 under the reaction conditions (Figure 8a). However, the catalytic activity was considerably affected by the reuse of the CuNi/TiO₂ and CuNi/C catalysts (Figure 8b,c). Benzyl alcohol conversion decreased from 54.9% to 23.7% in four consecutive runs over the CuNi/TiO₂ catalyst, whereas the selectivity toward benzaldehyde approximated 99% in the second, third, and fourth cycles (Figure 8b). A significant decrease was also observed in the conversion of benzyl alcohol from 64.3% to 12.2% for CuNi/C after four reaction cycles. The BET surface areas measured 1186.0, 15.2, and 94.9 m²/g for MIL-101, TiO₂, and C, respectively. Total pore volume reached 0.49, 0.014, and 0.11 cm³/g for MIL-101, TiO₂, and C, respectively. The large porous cavities of MIL-101 can be used to trap bimetallic Cu–Ni nanoparticles and inhibit nanoparticle leaching. CuNi/MIL-101 displayed better stability than the CuNi/TiO₂ and CuNi/C catalysts. The decline in the catalytic activity was possibly due to the leaching of metals (Cu and Ni) under experimental conditions (Figure 8b,c).

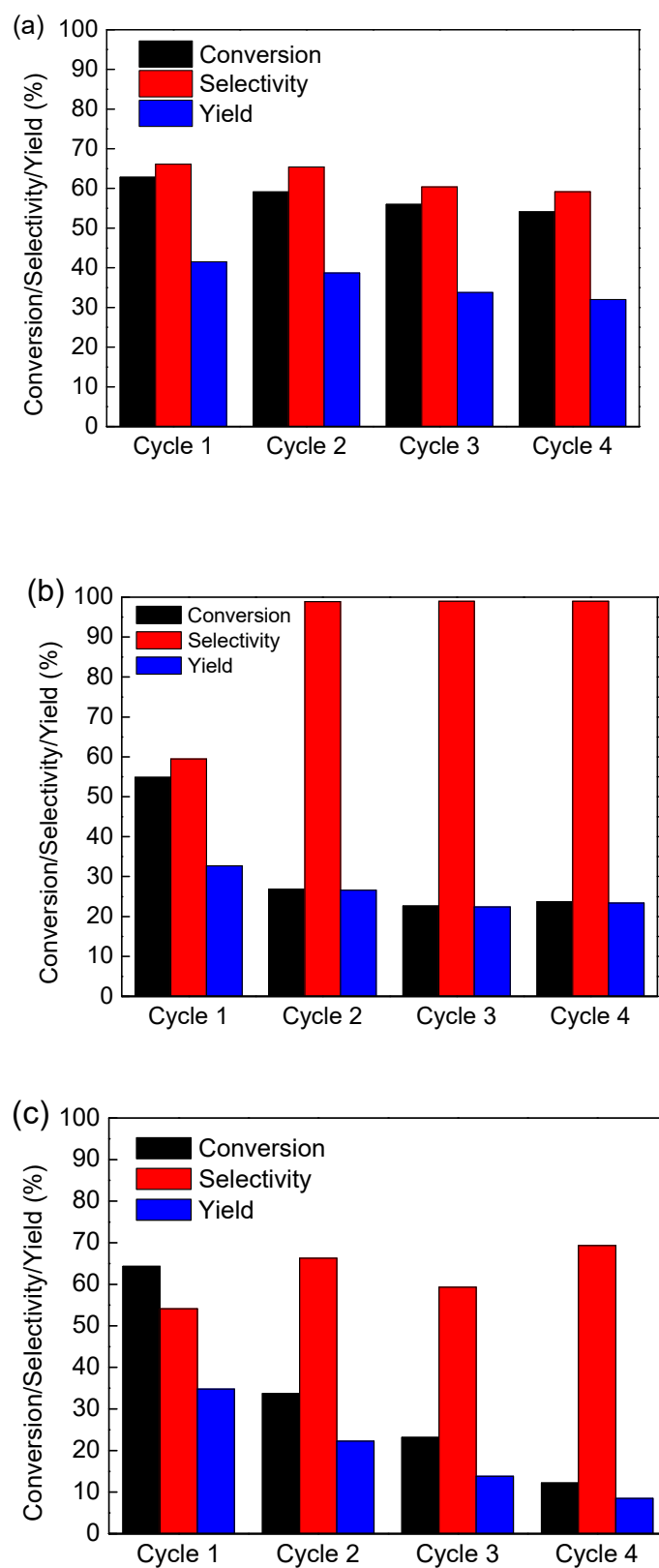


Figure 8. Recycling results of CuNi/MIL-101 (a), CuNi/TiO₂ (b), and CuNi/C (c) catalysts in the oxidation reaction of benzyl alcohol (reaction condition: 0.2 mmol of benzyl alcohol, 1.5 mL of THF, 0.04 g of catalyst, 100 °C, 5 bar, 4 h).

The stability of the Cu–Ni-supported catalysts was studied. The XRD patterns of fresh and recycled CuNi/MIL-101, CuNi/TiO₂, and CuNi/C are shown in Figure 9. The characteristic peak intensity of the recycled CuNi/MIL-101 decreased severely, suggesting that the structure of the recycled CuNi/MIL-101 was slightly destroyed during the oxidation of benzyl alcohol under present reaction conditions (Figure 9a). The XRD patterns of CuNi/TiO₂ and CuNi/C after four runs were similar to those of the as-prepared CuNi/TiO₂ and CuNi/C (Figure 9b,c). Such a similarity illustrates that recycled CuNi/TiO₂ and CuNi/C retained their structure integrity after four runs under the present reaction condition [43]. Figure 10 shows the N₂ adsorption–desorption isotherms for recycled CuNi/MIL-101, CuNi/TiO₂, and CuNi/C. All of the recycled catalysts displayed a type IV isotherm. The BET surface areas of the recycled CuNi/MIL-101, CuNi/TiO₂, and CuNi/C were 632.0, 7.2, 21.3 m²/g, respectively. The BET surface area decreased significantly for the recycled Cu–Ni-supported catalysts when compared with that of the as-prepared. The decrease in the BET surface area could be due to the collapse of the structure or/and the substrate/solvents blocking the pores of the support [10].

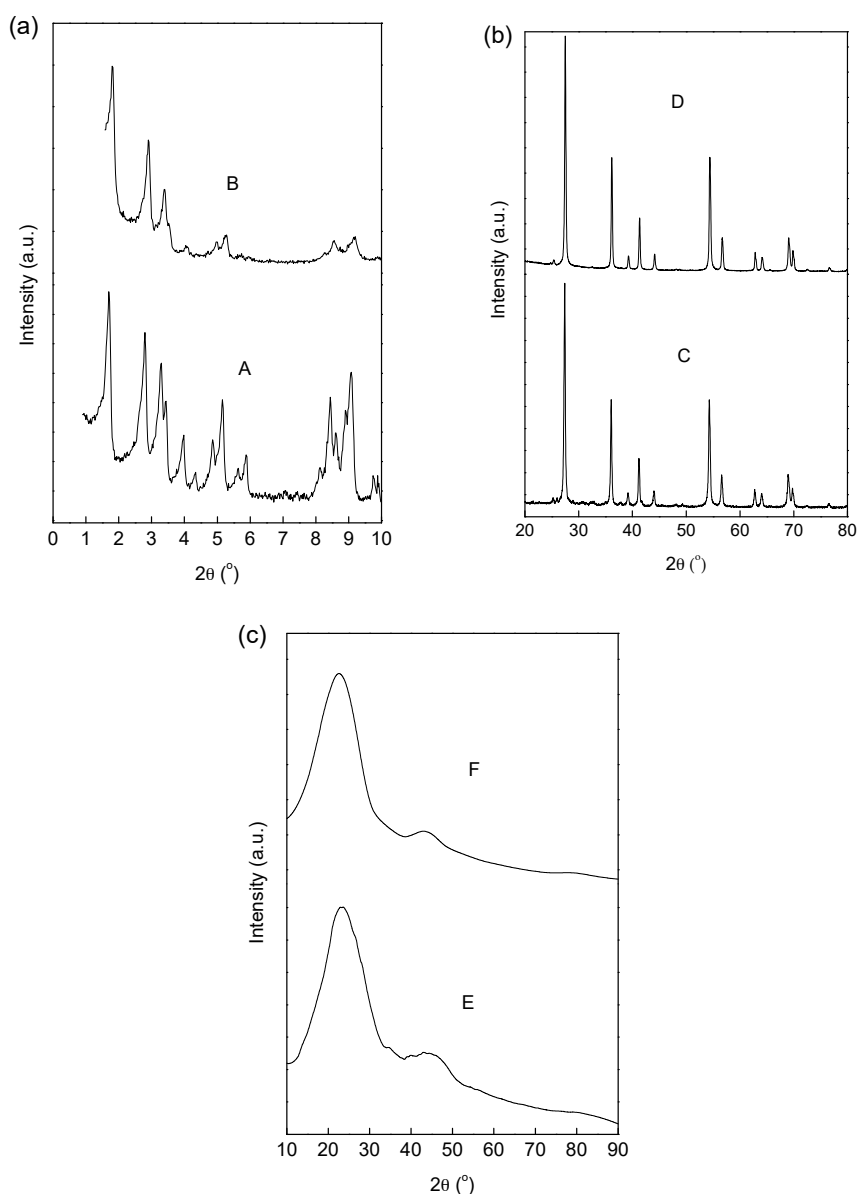


Figure 9. (a) XRD patterns of fresh (A) and recycled (B) CuNi/MIL-101; (b) XRD patterns of fresh (C) and recycled (D) CuNi/TiO₂; (c) XRD patterns of fresh (E) and recycled (F) CuNi/MIL-101.

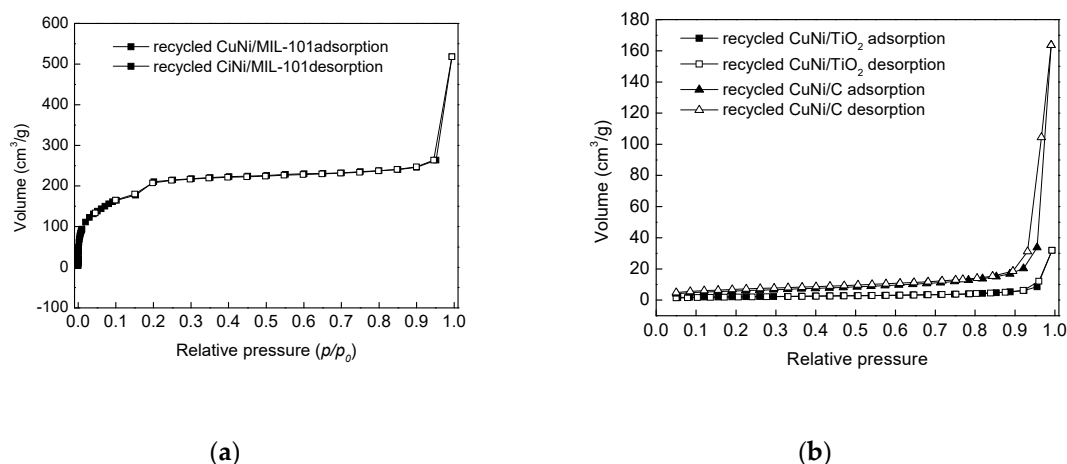


Figure 10. Nitrogen adsorption–desorption isotherms of the samples measured at 77 K: (a) recycled CuNi/MIL-101; (b) CuNi/TiO₂ and CuNi/C.

The leaching of the CuNi/MIL-101, CuNi/TiO₂, and CuNi/C catalysts was tested to further investigate the stability of the catalysts. This process was conducted by stopping the benzyl alcohol oxidation reaction after 2 h at 100 °C under 5 bar of O₂ using THF as the solvent and by separating the reaction mixture from the catalyst via centrifugation. Benzyl alcohol conversions reached 22.9%, 32.8%, and 31.9% at 100 °C under 5 bar of O₂ within 2 h over CuNi/MIL-101, CuNi/TiO₂, and CuNi/C, respectively. Furthermore, the reaction solution was reused and the entire reaction was continued for another 2 h under the same reaction conditions. Benzyl alcohol conversion increased by 4.8%, 14.6%, and 8.9% after reacting for another 2 h for CuNi/MIL-101, CuNi/TiO₂, and CuNi/C, respectively, thereby implying the leaching of active species after the removal of the solid catalyst. The Cu and Ni contents in the reaction solutions after removal of CuNi/MIL-101, CuNi/TiO₂, and CuNi/C were 0.00014 and 0.0024, 0.11 and 0.10, and 0.010 and 0.060 wt%, respectively, as determined by ICP-OES, which were consistent with the leaching results.

3. Materials and Methods

3.1. Materials

TiO₂ (rutile, 99.99%) was purchased from Macklin and used without further purification. C (99.5%, 30 nm), nickel nitrate hexahydrate (Ni(NO₃)₂·6H₂O, 99.99%), n-butanol (99.9%), 4-chlorobenzyl alcohol (98%), and 4-methoxybenzyl alcohol were supplied by Aladdin Reagent Co. Ltd. (Shanghai, China). Copper nitrate (Cu(NO₃)₂·3H₂O, 99%) and 4-methyl benzyl alcohol (99%) were obtained from Adamas-Beta Reagent Co. Ltd. (Shanghai, China). Benzyl alcohol, THF, and ethanol were obtained from Sinopharm Chemical Reagent Co. Ltd. (Beijing, China).

3.2. Preparation of Catalysts

MIL-101 was prepared following a method described in the literature [23]. Cu–Ni bimetallic catalysts were prepared by co-immobilization followed by H₂ reduction. A typical procedure for the preparation of the CuNi/MIL-101 catalyst is described as follows. First, Cu(NO₃)₂·3H₂O (0.4 mmol, 96.6 mg) and Ni(NO₃)₂·6H₂O (0.4 mmol, 116.3 mg) were dissolved in 2 mL ethanol. Subsequently, the solution was dropwise added to MIL-101 (0.5 g) and sonicated for 1 h in an ultrasonic cleaner. Finally, the mixture was left to stand for 12 h at room temperature, dried under vacuum for 8 h at 50 °C, and reduced at 50 °C in H₂ flow (12 mL/min) for 2 h. The obtained catalyst was labeled CuNi/MIL-101. CuNi/TiO₂ and CuNi/C catalysts were prepared using the same procedure, but differed due to changing the MIL-101 support to TiO₂ and C. The actual Cu and Ni contents in the CuNi/MIL-101, CuNi/TiO₂, and CuNi/C catalysts were 3.15 and 2.80, 3.53 and 3.46, and 2.62 and 2.33 wt%, respectively,

as determined by inductively coupled plasma (ICP) optical emission spectroscopy. Four different bimetallic Cu:Ni catalysts supported on MIL-101 were also prepared by co-immobilization followed by H₂ reduction, with a total metal loading of ca. 6%. The as-synthesized catalysts were labelled as Cu(3)Ni/MIL-101, Cu(2)Ni/MIL-101, CuNi(2)/MIL-101, and CuNi(3)/MIL-101 on the basis of the mole ratio of Cu and Ni.

3.3. Catalyst Characterization

The details of the characterizations with XRD, XPS, nitrogen adsorption/desorption, and ICP atomic emission spectroscopy analysis are the same as those in our previous work [10]. TEM images were recorded with a Jeol JEM-1210 transmission electron microscope (Jeol, Tokyo, Japan) with a high-angle annular dark-field detector. EDS line-scanning profile analysis was performed on an Oxford X-MaxN 80T IE250 spectroscopy instrument (Oxford, UK). NH₃-TPD analyses of MIL-101, TiO₂, and C supports were conducted on a MicrotracBEL AutoChem BELCAT II Chemisorption Analyzer (Bel, Osaka, Japan).

3.4. Selective Oxidation of Benzyl Alcohol

Selective oxidation of benzyl alcohol with molecular oxygen was conducted in a stainless-steel high-pressure reactor equipped with magnetic stirring and a temperature controller under mild conditions. In a typical experiment, 0.2 mmol benzyl alcohol, 40 mg catalyst, and 1.5 mL solvent were mixed in a 10 mL stainless-steel high-pressure reactor. The system was pumped five times with pure O₂ to remove air prior to the reaction. Subsequently, the reactor was immersed in a methylsilicon oil bath at 100 °C under 5 bar of O₂ to initiate the reaction. After the reaction, the mixture was centrifuged to remove the catalyst particles completely. The remaining solution was analyzed with a gas chromatograph (GC-6890, Purkinje General instrument Co., Ltd., Beijing, China) equipped with a SE-54 capillary column and flame ionization detector. Reaction products were identified by comparison with known standard samples, and an external standard method was used for the qualitative analysis of the amounts of the reactants consumed (conversion) and products generated (selectivity). In the recycling experiment, the catalysts were separated from the mixture by centrifugation after each run, and washed with ethanol twice. Finally, the catalysts were dried at 50 °C for 4 h in a vacuum at 0.1 MPa for the next reaction.

4. Conclusions

A series of bimetallic Cu–Ni nanoparticles supported on MIL-101, TiO₂, and C was successfully prepared using co-immobilization followed by H₂ reduction for the selective oxidation of benzyl alcohol to benzaldehyde using molecular oxygen as the oxidizing agent. The acidity of the supports and Cu:Ni mole ratios substantially influenced the catalytic performance of the oxidation of benzyl alcohol into benzaldehyde. The CuNi/MIL-101 catalyst possessing more acid sites showed the highest yield for the selective oxidation of benzyl alcohol to the corresponding aldehyde at 100 °C. Additionally, the CuNi/MIL-101 catalyst exhibited a high functional group (electron-donating and electron-withdrawing groups) tolerance. The CuNi/MIL-101 catalyst also displayed better stability than the CuNi/TiO₂ and CuNi/C catalysts due to the large porous cavities of the MIL-101 support. These findings emphasize the potential of developing new heterogeneous catalytic systems for the oxidation of benzyl alcohol under mild conditions.

Author Contributions: Conceptualization, Methodology and Writing—original draft preparation, L.L. (Lili Liu) and X.T.; Investigation—experiments and analyses, S.J., Y.L., L.G., and S.Y.; Writing—review and editing, X.Z. and L.L. (Li Liu).

Funding: This research was funded by the National Natural Science Foundation of China (grant number 21802104) and the Natural Science Foundation of Shandong Province (grant number ZR2017MB056).

Conflicts of Interest: The authors declare no conflict of interest.

References

1. Gong, X.; Liu, B.; Zhang, G.; Xu, G.; Zhao, T.; Shi, D.; Wang, Q.; Zhang, J. A mild and environmentally benign strategy towards hierarchical CeO₂/Au nanoparticle assemblies with crystal facet-enhanced catalytic effects for benzyl alcohol aerobic oxidation. *CrystEngComm* **2016**, *18*, 5110–5120. [[CrossRef](#)]
2. Harada, T.; Ikeda, S.; Hashimoto, F.; Sakata, T.; Ikeue, K.; Torimoto, T.; Matsumura, M. Catalytic activity and regeneration property of a Pd nanoparticle encapsulated in a hollow porous carbon sphere for aerobic alcohol oxidation. *Langmuir* **2010**, *26*, 17720–17725. [[CrossRef](#)] [[PubMed](#)]
3. Možina, Š.; Stavber, S.; Iskra, J. Dual catalysis for the aerobic oxidation of benzyl alcohols-nitric acid and fluorinated alcohol. *Eur. J. Org. Chem.* **2017**, *3*, 448–452. [[CrossRef](#)]
4. Sun, J.Y.; Han, Y.X.; Fu, H.Y.; Qu, X.L.; Xu, Z.Y.; Zheng, S.R. Au@Pd/TiO₂ with atomically dispersed Pd as highly active catalyst for solvent-free aerobic oxidation of benzyl alcohol. *Chem. Eng. J.* **2017**, *313*, 1–9. [[CrossRef](#)]
5. Tian, J.; Li, J.; Wei, N.; Xu, X.; Cui, H.; Liu, H. Ru nanoparticles decorated TiO₂ nanobelts: A heterostructure towards enhanced photocatalytic activity and gas-phase selective oxidation of benzyl alcohol. *Ceram. Int.* **2016**, *42*, 1611–1617. [[CrossRef](#)]
6. Meng, Y.Y.; An, Q.D.; Xiao, Z.Y.; Zhai, S.R.; Shi, Z. Pd NPs supported on N-doped carbon layer coated ZrSBA-15 for efficient heterogeneous catalysis reactions. *Microporous Mesoporous Mater.* **2018**, *266*, 64–74. [[CrossRef](#)]
7. Sun, J.Y.; Tong, X.L.; Liu, Z.H.; Liao, S.Y.; Zhang, X.L.; Xue, S. Gold-catalyzed selectivity-switchable oxidation of benzyl alcohol in the presence of molecular oxygen. *Catal. Commun.* **2016**, *85*, 70–74. [[CrossRef](#)]
8. Chen, L.J.; Yan, J.Q.; Tong, Z.X.; Yu, S.Y.; Tang, J.T.; Ou, B.L.; Yue, L.J.; Tian, L. Nanofiber-like mesoporous alumina supported palladium nanoparticles as a highly active catalyst for base-free oxidation of benzyl alcohol. *Microporous Mesoporous Mater.* **2018**, *266*, 126–131. [[CrossRef](#)]
9. Alshammari, H.; Alhumaimess, M.; Alotaibi, M.H.; Alshammari, A.S. Catalytic activity of bimetallic AuPd alloys supported MgO and MnO₂ nanostructures and their role in selective aerobic oxidation of alcohols. *J. King Saud Univ. Sci.* **2017**, *29*, 561–566. [[CrossRef](#)]
10. Liu, L.L.; Zhou, X.J.; Yan, Y.M.; Zhou, J.; Zhang, W.P.; Tai, X.S. Bimetallic Gold-Silver Nanoparticles Supported on Zeolitic Imidazolate Framework-8 as Highly Active Heterogeneous Catalysts for Selective Oxidation of Benzyl Alcohol into Benzaldehyde. *Polymers* **2018**, *10*, 1089. [[CrossRef](#)]
11. Liu, L.L.; Tai, X.S.; Zhou, X.J.; Hou, J.X.; Zhang, Z.H. Bimetallic AuNi alloy nanoparticles in a metaleorganic framework (MIL-101) as efficient heterogeneous catalysts for selective oxidation of benzyl alcohol into benzaldehyde. *J. Alloy. Compd.* **2019**, *790*, 326–336. [[CrossRef](#)]
12. Cruz, P.; Pérez, Y.; Hierro, I.D.; Fajardo, M. Copper, copper oxide nanoparticles and copper complexes supported on mesoporous SBA-15 as catalysts in the selective oxidation of benzyl alcohol in aqueous phase. *Microporous Mesoporous Mater.* **2016**, *220*, 136–147. [[CrossRef](#)]
13. Fu, X.; Wu, S.; Li, Z.; Yang, X.; Wang, X.; Peng, L.; Hu, J.; Huo, Q.; Guan, J.; Kan, Q. Highly efficient Ni-Co oxide nanoparticles on nitrogen-doped FDU-15 for aerobic benzyl alcohol oxidation. *RSC Adv.* **2016**, *6*, 57507–57513. [[CrossRef](#)]
14. Kimi, M.; Jaidie, M.M.H.; Pang, S.C. Bimetallic Cu-Ni nanoparticles supported on activated carbon for catalytic oxidation of benzyl alcohol. *J. Phys. Chem. Solids* **2018**, *112*, 50–53. [[CrossRef](#)]
15. Chen, G.J.; Wang, J.S.; Jin, F.Z.; Liu, M.Y.; Zhao, C.W.; Li, Y.A.; Dong, Y.B. Pd@Cu(II)-MOF-catalyzed aerobic oxidation of benzylic alcohols in air with high conversion and selectivity. *Inorg. Chem.* **2016**, *55*, 3058–3064. [[CrossRef](#)]
16. Kumar, A.; Gautam, R.K.; Belwal, M. Synthesis and characterization of Au/γ-Al₂O₃ nanocatalysts for vapor-phase selective oxidation of benzyl alcohol under aerobic condition. *Curr. Catal.* **2018**, *7*, 35–42. [[CrossRef](#)]
17. Tareq, S.S.; Saiman, M.I.; Hin, T.Y.Y.; Abdullah, A.H.; Rashid, U. The impact of hydrogen peroxide as an oxidant for solvent-free liquid phase oxidation of benzyl alcohol using Au-Pd supported carbon and titanium catalysts. *Bull. Chem. React. Eng. Catal.* **2018**, *13*, 373–385. [[CrossRef](#)]
18. Cordoba, M.; Miranda, C.; Lederhos, C.; Coloma-Pascual, F.; Ardila, A.; Fuentes, G.A.; Pouilloux, Y.; Ramírez, A. Catalytic performance of Co₃O₄ on different activated carbon supports in the benzyl alcohol oxidation. *Catalysts* **2017**, *7*, 384. [[CrossRef](#)]

19. Liu, L.L.; Tai, X.S.; Zhou, X.J. Au³⁺/Au⁰ supported on chromium(III) terephthalate metal organic framework (MIL-101) as an efficient heterogeneous catalyst for three-component coupling synthesis of propargylamines. *Materials* **2017**, *10*, 89.
20. Gil, S.; Garcia-Vargas, J.M.; Liotta, L.F.; Pantaleo, G.; Ousmane, M.; Retailleau, L.; Giroir-Fendler, A. Catalytic oxidation of propene over Pd catalysts supported on CeO₂, TiO₂, Al₂O₃ and M/Al₂O₃ oxides (M = Ce, Ti, Fe, Mn). *Catalysts* **2015**, *5*, 671–689. [[CrossRef](#)]
21. Watanabe, M.; Aizawa, Y.; Iida, T.; Nishimura, R.; Inomata, H. Catalytic glucose and fructose conversions with TiO₂ and ZrO₂ in water at 473 K: Relationship between reactivity and acid–base property determined by TPD measurement. *Appl. Catal. A Gen.* **2005**, *295*, 150–156. [[CrossRef](#)]
22. Liu, L.; Tai, X.; Liu, J.; Li, D.; Zhou, X.; Zhang, L.; Wei, X. Preparation of propargylamines catalyzed by heterogeneous catalysts with double catalytic sites. *Chem. J. Chin. Univ.-Chin.* **2018**, *39*, 482–490.
23. Sun, Y.; Zhang, G.; Liu, J.; Zhao, P.; Hou, P.; Xu, Y.; Zhang, R. Effect of different activated carbon support on CH₄–CO₂ reforming over Co-based catalysts. *Int. J. Hydrog. Energy* **2018**, *43*, 1497–1507. [[CrossRef](#)]
24. Harisekhar, M.; Pavan Kumar, V.; Shanthi Priya, S.; Chary, K.V.R. Vapour phase hydrogenolysis of glycerol to propanediols over Cu/SBA-15 catalysts. *J. Chem. Technol. Biotechnol.* **2015**, *90*, 1906–1917. [[CrossRef](#)]
25. Jiang, H.; Wang, Q.; Wang, H.; Chen, Y.; Zhang, M. MOF-74 as an efficient catalyst for the low-temperature selective catalytic reduction of NO_x with NH₃. *ACS Appl. Mater. Interfaces* **2016**, *8*, 26817–26826. [[CrossRef](#)]
26. Qiu, J.H.; Zhang, X.G.; Xie, K.L.; Zhang, X.F.; Feng, Y.; Jia, M.M.; Yao, J.F. Noble metal nanoparticle-functionalized Zr-metal organic frameworks with excellent photocatalytic performance. *J. Colloid Interface Sci.* **2019**, *538*, 569–577. [[CrossRef](#)] [[PubMed](#)]
27. Chen, D.; Yang, D.; Dougherty, C.A.; Lu, W.; Wu, H.; He, X.; Cai, T.; Van Dort, M.E.; Ross, B.D.; Hong, H. In vivo targeting and positron emission tomography imaging of tumor with intrinsically radioactive metal-organic frameworks nanomaterials. *ACS Nano* **2017**, *11*, 4315–4327. [[CrossRef](#)] [[PubMed](#)]
28. Akel, S.; Dillert, R.; Balayeva, N.O.; Boughaled, R.; Koch, J.; Azzouzi, M.E.; Bahnemann, D.W. Ag/Ag₂O as a Co-catalyst in TiO₂ photocatalysis: Effect of the Co-catalyst/photocatalyst mass ratio. *Catalysts* **2018**, *8*, 647. [[CrossRef](#)]
29. Salmasi, M.; Fatemi, S.; Mortazavi, Y. Fabrication of promoted TiO₂ nanotubes with superior catalytic activity against TiO₂ nanoparticles as the catalyst of oxi-desulfurization process. *J. Ind. Eng. Chem.* **2016**, *39*, 66–76. [[CrossRef](#)]
30. Chen, J.; Zhang, J.; Jiang, Y.; Yang, L.; Zhong, J.; Wang, G.; Wang, R. Enhanced formic acid electro-oxidation reaction on ternary Pd–Ir–Cu/C catalyst. *Appl. Surf. Sci.* **2015**, *357*, 994–999. [[CrossRef](#)]
31. Kang, W.D.; Wei, Y.C.; Liu, C.W.; Wang, K.W. Enhancement of electrochemical properties on Pd–Cu/C electrocatalysts toward ethanol oxidation by atmosphere induced surface and structural alteration. *Electrochem. Commun.* **2011**, *13*, 162–165. [[CrossRef](#)]
32. Nam, K.M.; Park, H.K.; Lee, C. Synthesis and electrochemical properties of carbon nanofibers and SiO₂/carbon nanofiber composite on Ni–Cu/C-fiber textiles. *J. Nanosci. Nanotechnol.* **2015**, *15*, 8989–8995. [[CrossRef](#)] [[PubMed](#)]
33. Karaca, H.; Safonova, O.V.; Chambrey, S.; Fongarland, P.; Roussel, P.; Constant, A.G.; Lacroix, M.; Khodakov, A.Y. Structure and catalytic performance of Pt-promoted alumina-supported cobalt catalysts under realistic conditions of Fischer–Tropsch synthesis. *J. Catal.* **2011**, *277*, 14–26. [[CrossRef](#)]
34. Pieta, I.S.; Rathi, A.; Pieta, P.; Nowakowski, R.; Hołdyski, M.; Pisarek, M.; Kaminska, A.; Gawande, M.B.; Zboril, R. Electrocatalytic methanol oxidation over Cu, Ni and bimetallic Cu–Ni nanoparticles supported on graphitic carbon nitride. *Appl. Catal. B Environ.* **2019**, *244*, 272–283. [[CrossRef](#)]
35. Duan, H.; Li, Y.; Lv, X.; Chen, D.; Long, M.; Wen, L. CuO–ZnO anchored on APS modified activated carbon as an enhanced catalyst for methanol synthesis—the role of ZnO. *J. Mater. Res.* **2018**, *33*, 1–7. [[CrossRef](#)]
36. Sun, B.; Li, H.; Li, X.; Liu, X.; Zhang, C.; Xu, H.; Zhao, X.S. Degradation of organic dyes over fenton-like Cu₂O–Cu/C catalysts. *Ind. Eng. Chem. Res.* **2018**, *57*, 14011–14021. [[CrossRef](#)]
37. De Godoi, F.C.; Rodriguez-Castellon, E.; Guibal, E.; Beppu, M.M. An XPS study of chromate and vanadate sorption mechanism by chitosan membrane containing copper nanoparticles. *Chem. Eng. J.* **2013**, *234*, 423–429. [[CrossRef](#)]
38. Liu, L.J.; Lou, H.; Chen, M. Selective hydrogenation of furfural to tetrahydrofurfuryl alcohol over Ni/CNTs and bimetallic CuNi/CNTs catalysts. *Int. J. Hydrog. Energy* **2016**, *41*, 14721–14731. [[CrossRef](#)]

39. Liu, G.Q.; Zhang, X.; Zhao, C.J.; Xiong, Q.Z.; Gong, W.B.; Wang, G.Z.; Zhang, Y.X.; Zhan, H.M.; Zhao, H.J. Electrocatalytic oxidation of benzyl alcohol for simultaneously promoting H₂ evolution by a Co_{0.83}Ni_{0.17}/activated carbon electro-catalyst. *New J. Chem.* **2018**, *42*, 6381–6388. [[CrossRef](#)]
40. Liu, M.; Fan, G.; Yu, J.; Yang, L.; Li, F. Defect-rich Ni–Ti layered double hydroxide as a highly efficient support for Au nanoparticles in base-free and solvent-free selective oxidation of benzyl alcohol. *Dalton Trans.* **2018**, *47*, 5226–5235. [[CrossRef](#)]
41. Cui, W.; Xiao, Q.; Sarina, S.; Ao, W.; Xie, M.; Zhu, H.; Bao, Z. Au–Pd alloy nanoparticle catalyzed selective oxidation of benzyl alcohol and tandem synthesis of imines at ambient conditions. *Catal. Today* **2014**, *235*, 152–159. [[CrossRef](#)]
42. Gao, F.; Goodman, D.W. Pd–Au bimetallic catalysts: Understanding alloy effects from planar models and (supported) nanoparticles. *Chem. Soc. Rev.* **2012**, *41*, 8009–8020. [[CrossRef](#)] [[PubMed](#)]
43. Liu, L.L.; Tai, X.S.; Zhang, N.N.; Meng, Q.G.; Xin, C.L. Supported Au/MIL-53(Al): A reusable green solid catalyst for the three-component coupling reaction of aldehyde, alkyne, and amine. *React. Kinet. Mech. Catal.* **2016**, *119*, 335–348. [[CrossRef](#)]



© 2019 by the authors. Licensee MDPI, Basel, Switzerland. This article is an open access article distributed under the terms and conditions of the Creative Commons Attribution (CC BY) license (<http://creativecommons.org/licenses/by/4.0/>).